Distinct Acetate Utilization Strategies Differentiate Butyrate and Medium-Chain Carboxylic Acid Producing Chain-Elongating Bacteria

Ian M. Gois[#], Connor M. Bowers[#], Byung-Chul Kim, Robert Flick, Christopher E. Lawson*

Department of Chemical Engineering & Applied Chemistry, University of Toronto, Toronto, ON M5T 3E5, Canada.

# These authors contributed equally to this work

* Correspondence: chris.lawson@utoronto.ca

Abstract

Chain elongating bacteria (CEB) are a unique guild of anaerobes that upcycle organic waste into valuable short- and medium-chain carboxylic acids (MCCAs), enabling a circular bioeconomy. However, the metabolic rules that determine product chain length have remained elusive. Here, we combine ^{13}C isotope tracing, proteomics, enzyme assays, and metabolic modelling to show that distinct acetate utilization strategies underlie the divergence between butyrate- and MCCA-producing CEB. MCCA-producing strains recycle acetate to maximize lactate use under acetate limitation, but at the cost of slower growth. In contrast, butyrate-producing strains grow faster by favoring acetate assimilation, at the cost of restricted lactate utilization when acetate is scarce. These physiological trade-offs are encoded in the substrate specificity of coenzyme A transferase, the terminal enzyme in reverse β-oxidation. Our findings uncover a fundamental constraint shaping chain-length selectivity in CEB and offer new strategies to optimize MCCA production from organic waste streams.

Introduction

Anaerobic fermentation could transform billions of tons of organic waste per year into economically viable, carbon-negative fuels and chemicals, enabling a circular bioeconomy. One promising approach is microbial chain elongation, which produces C_6-C_8 medium chain carboxylic acids (MCCAs)[1]. These versatile platform chemicals can be applied directly in agricultural feeds, nutritional supplements, cosmetics, antimicrobials and surfactants[2,3], or derivatized to produce liquid fuels[4–6], polyhydroxyalkanoates[7], and other oleochemicals such as alcohols, diols and dicarboxylates[8,9]. Because most MCCAs are currently sourced from palm kernel and coconut oil[1], local production via waste fermentation offers additional environmental benefit by mitigating deforestation and biodiversity loss.

MCCAs are produced by chain elongating bacteria (CEB), a unique guild of strict anaerobes first described by Barker in 1939 with the isolation of *Clostridium kluyveri*[10]. A key challenge in deploying chain elongation industrially has been controlling product distribution. While all known CEB synthesize butyrate (C4), hexanoate (C6) and/or octanoate (C8) via the reverse beta-oxidation (RBO) pathway[11], the relative abundance of different chain length carboxylates varies drastically among species and environmental conditions. For example, some CEB only produce butyrate, including many abundant in the human gut[12,13], whereas others produce a substantial amount of hexanoate and octanoate, despite using the same RBO pathway to elongate carbon chains[14–16]. Understanding the ecological and physiological principles that drive some CEB to produce MCCAs rather than only butyrate is therefore essential for improving the yield, selectivity and productivity of MCCA bioprocesses[11].

During RBO, an electron donor such as lactate is oxidized to acetyl-CoA, which then condenses with an acyl-CoA to initiate a new chain elongation cycle (Figure 1). The resulting intermediate passes through a series of reduction and dehydration steps, elongating the carbon chain by two carbons each cycle. Termination of chain elongation is typically catalyzed by a CoA transferase (CoAT), which transfers CoA

62 from the final acyl-CoA to acetate, yielding a free carboxylic acid (i.e., butyrate,
63 hexanoate, or octanoate) and regenerating acetyl-CoA[17]. Despite a general
64 understanding of RBO, how acetate is used in the pathway and its implications for
65 energy conservation have been debated. Early work by Barker proposed that the
66 acetyl-CoA produced by termination enters the RBO cycle, and energy is conserved
67 via a then-unknown chemiosmotic mechanism. We call this stoichiometry *acetate*
68 *assimilation*, because it leads to net acetate consumption*:*
69

70 $$1\ Lactate + 1\ Acetate \rightarrow 1\ Butyrate + 1\ CO_2 + 1\ H_2O \quad (Eq.\ 1)$$

71 $$2\ Lactate + 1\ Acetate \rightarrow 1\ Hexanoate + 2\ CO_2 + 2\ H_2O \quad (Eq.\ 2)$$

72 $$3\ Lactate + 1\ Acetate \rightarrow 1\ Octanoate + 3\ CO_2 + 3\ H_2O \quad (Eq.\ 3)$$

73

74 In Barker's work, the organism under study, *Clostridium kluyveri*, consumed ethanol
75 rather than lactate as its electron donor, but both substrates yield two molecules of
76 NADH when oxidized to acetyl-CoA and therefore follow similar overall
77 stoichiometry. Later, Thauer and colleagues proposed that not all product formation
78 requires net acetate consumption[18–20]. Instead of entering the RBO cycle, some acetyl-
79 CoA is diverted by phosphate acetyltransferase (PTA) and acetate kinase (ACK) to
80 regenerate acetate, while producing ATP via substrate-level phosphorylation (SLP)[11].
81 We call this stoichiometry *acetate recycling:*
82

83 $$2\ Lactate \rightarrow 1\ Butyrate + 2\ CO_2 + 2\ H_2 \quad (Eq.\ 4)$$

84 $$3\ Lactate \rightarrow 1\ Hexanoate + 3\ CO_2 + 2\ H_2 + 1\ H_2O \quad (Eq.\ 5)$$

85 $$4\ Lactate \rightarrow 1\ Octanoate + 4\ CO_2 + 2\ H_2 + 2\ H_2O \quad (Eq.\ 6)$$

86

87 Barker's hypothesis was later supported–ironically by Thauer *et al.*–with the
88 discovery of chemiosmotic energy conservation in *C. kluyveri*[21–24]. The reduction of an
89 enoyl-CoA is coupled to the reduction of ferredoxin via electron bifurcation, then
90 reduced ferredoxin is oxidized via the membrane bound ferredoxin:NAD^+
91 oxidoreductase (RNF complex) which generates ion motive force (IMF) for ATP

synthesis by ATPase[21,22] (Fig. 1). As a result, it is now widely accepted that CEB conserve energy through a combination of both chemiosmosis and substrate-level phosphorylation, with chemiosmosis generally assumed to dominate[2,3,11,21,23,24]. However, this has not been systematically tested across species and growth conditions.

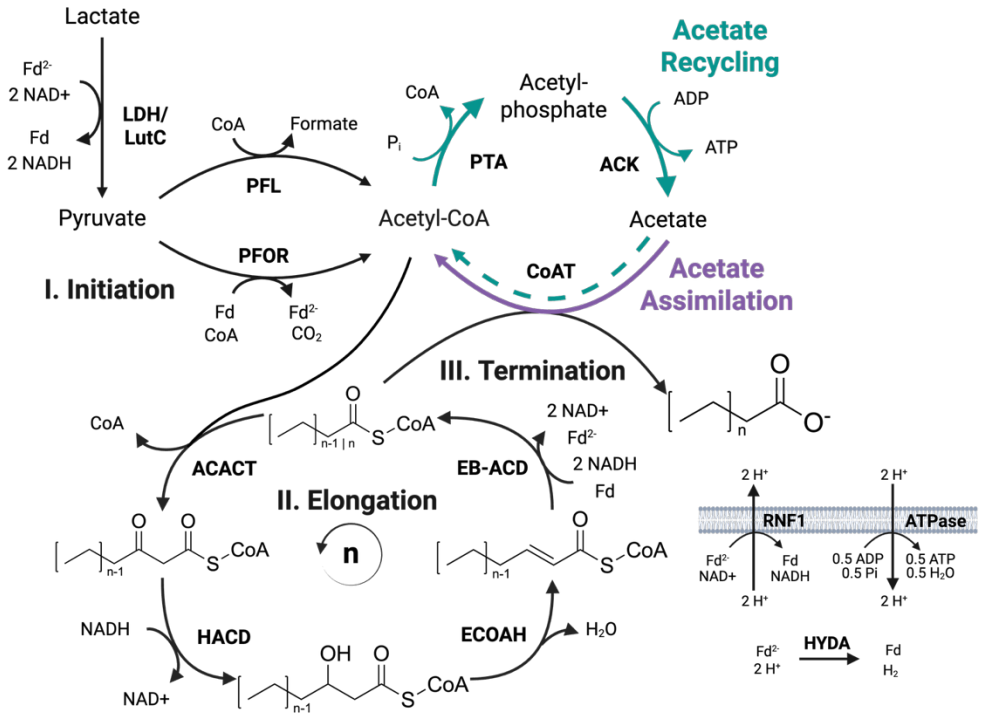

Figure 1. Butyrate (n=1), hexanoate (n=2) and octanoate (n=3) production from lactate. Initiation (I) generates acetyl-CoA via lactate oxidation. Acetyl-CoA is condensed with an acyl-CoA to form a lengthened carbon chain that is reduced and dehydrated during elongation (II) via the RBO cycle. The cycle is terminated (III) by a CoA transferase (CoAT), which transfers CoA from the final acyl-CoA to acetate to form a free carboxylic acid and regenerate acetyl-CoA. Acetyl-CoA may re-enter RBO, resulting in net acetate consumption (acetate assimilation) and energy conservation by chemiosmosis through the RNF complex. Alternatively, acetyl-CoA can be diverted through phosphate acetyltransferase (PTA) and acetate kinase (ACK) to regenerate acetate and conserve energy through substrate level phosphorylation (SLP). Purple arrow indicate reactions leading to acetate assimilation. Green arrows indicate reactions leading to acetate recycling. Biorender.com/wsekjeu.

Here, we combine batch fermentations, ^{13}C isotope tracing, proteomics, enzyme assays, and metabolic modelling to investigate the relationship between acetate metabolism and product formation in a butyrate-producing CEB (*Anaerostipes caccae*) and a MCCA-producing CEB (*Pseudoramibacter alactolyticus*). Our results suggest that

114 acetate utilization strategy differentiates MCCA-producing and butyrate-producing
115 CEB. We show that MCCA production allows for increased acetate recycling by
116 maintaining redox balance. This enables more lactate utilization under acetate-
117 limiting conditions, at the cost of slower growth due to an increased protein burden
118 associated with producing longer products. In contrast, exclusive butyrate production
119 enables faster growth due to a reduced catabolic protein demand, but constrains
120 acetate recycling, resulting in poor lactate utilization and growth under acetate
121 limiting conditions. This trade-off is reflected by differing substrate chain-length
122 specificities of CoAT in MCCA and butyrate producers. Together, these findings
123 provide foundational insights into chain-length selectivity of CEB and offer new
124 strategies to enhance MCCA production from waste.
125

126 # Results

127 ***P. alactolyticus* maintains growth and lactate consumption during acetate scarcity,**
128 **producing longer chain-length products**
129

130 *A. caccae* and *P. alactolyticus* are CEB of great interest. *A. caccae* is an important butyrate
131 producer in the human gut[13,25–27], and the genus *Pseudoramibacter* is often observed in
132 chain elongation bioreactors producing MCCAs[17,28–33]. To evaluate how acetate
133 availability affects growth, product formation and substrate utilization in *A. caccae*
134 *and P. alactolyticus,* we conducted lactate batch fermentations with and without
135 acetate. When acetate was supplemented, *A. caccae* only produced butyrate while *P.*
136 *alactolyticus* produced butyrate and hexanoate, and effectively all lactate was
137 consumed by both organisms. Interestingly, acetate consumption by *P. alactolyticus*
138 was significantly inferior to consumption by *A. caccae*. When lactate was provided and
139 acetate was not supplemented, *A. caccae* did not display significant growth. *P.*
140 *alactolyticus* grew and fully consumed lactate, albeit at a slower rate than with acetate,
141 and carboxylic acid production shifted towards hexanoate and octanoate (Fig. 2a).
142 Hence, acetate appears to be a mandatory co-substrate for *A. caccae* but a facultative
143 one for *P. alactolyticus*.

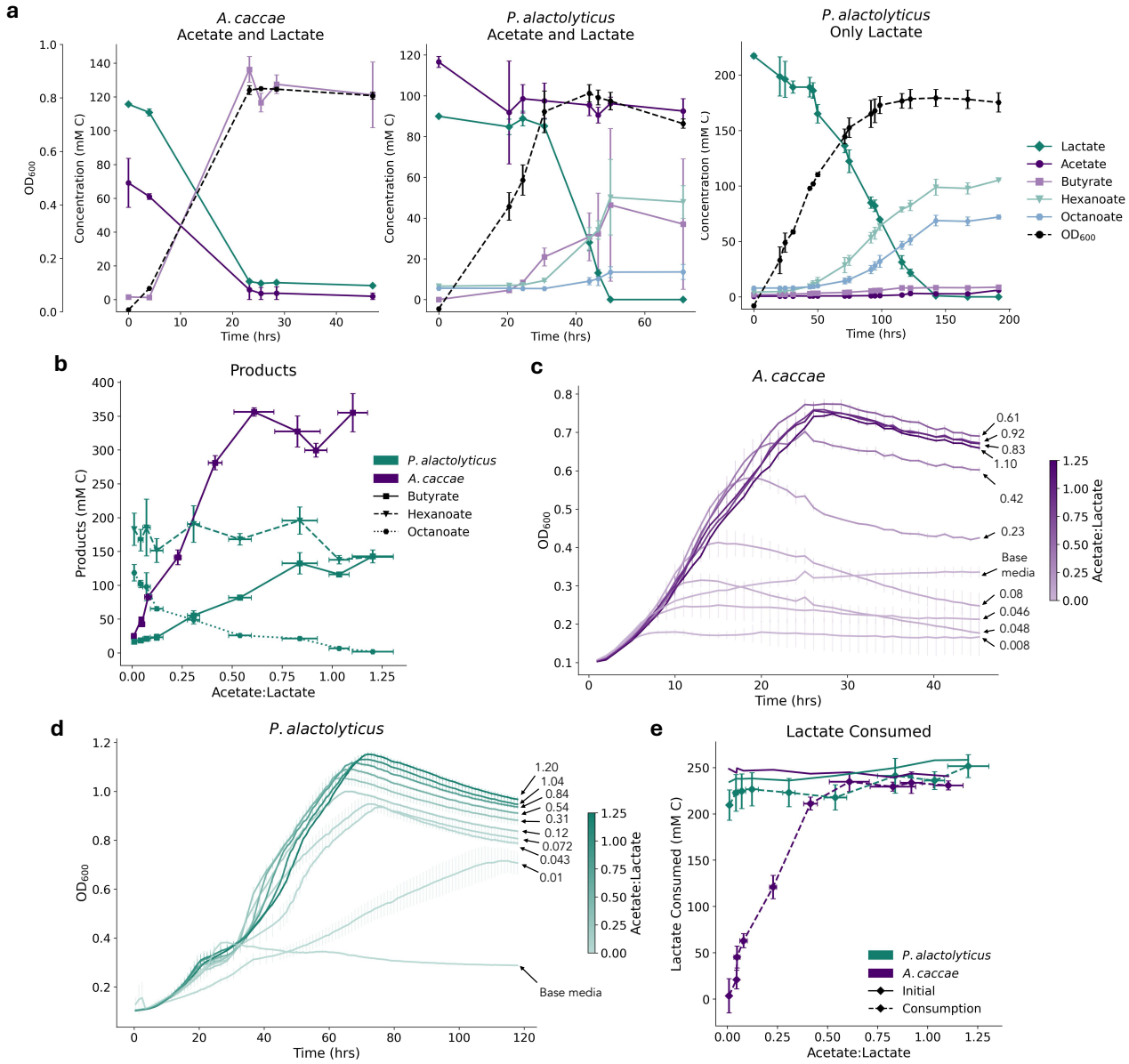

Figure 2. Batch experiments show effects of acetate-to-lactate ratio on carboxylic acid profile, growth and lactate utilization in *A. caccae* and *P. alactolyticus*. **a.** Substrate and product concentrations and growth throughout batch fermentation of *A. caccae* and *P. alactolyticus* on lactate and acetate, and of *P. alactolyticus* on lactate only (n = 3). **b.** Endpoint concentrations of butyrate, hexanoate and octanoate produced by both organisms at different acetate-to-lactate ratios (n = 3). *P. alactolyticus* favours hexanoate and octanoate production as ratio decreases, *A. caccae* solely produces butyrate. Error bars represent 1 standard deviation. **c.** Growth curves of *A. caccae* and **d.** *P. alactolyticus* at varied acetate-to-lactate ratios (lactate concentration fixed at 100 mM) (n = 3). **e.** *P. alactolyticus* maintains growth and lactate consumption at low ratios, whereas these are severely hindered in *A. caccae*. Initial lactate concentrations and lactate consumed (initial minus endpoint concentration) by both organisms at different acetate-to-lactate ratios (n = 3). Base media condition does not contain lactate or acetate supplemented.

158 We then evaluated differences in these organisms' responses to intermediate acetate-
159 to-lactate ratios through batch cultures with acetate concentrations varying between
160 5 mM and 120 mM and a constant lactate concentration of 100 mM. Whereas *A. caccae*
161 only produced butyrate in all conditions, with production increasing with acetate
162 availability, *P. alactolyticus* produced a mixture of butyrate, hexanoate and octanoate,
163 favouring longer products at low acetate-to-lactate ratios (Fig. 2b). Lengthening of
164 products in response to acetate scarcity is reminiscent of similar observations in other
165 MCCA-producing CEB and bioreactors[10,11,34–36].
166
167 *A. caccae* growth decreased significantly as acetate supplementation was reduced (Fig.
168 2c, Supplementary Material Fig. 1b). On the other hand, *P. alactolyticus* maintained a
169 relatively constant maximum OD as acetate decreased (Fig. 2d, Supplementary
170 Material Fig. 1a). Consistent with these observations, lactate consumption by *A. caccae*
171 was poor at low acetate-to-lactate ratios and did not approach the amount available
172 in the media until a ratio of 0.5, while lactate was effectively fully consumed by *P.*
173 *alactolyticus* at all tested ratios (Fig. 2e). This confirms that *A. caccae* depends more
174 strongly on acetate than *P. alactolyticus*.
175
176 Unexpectedly, we observed minor growth on rich base media without lactate or
177 acetate supplementation (Fig. 2c,d). This is likely due to trace amounts of lactate and
178 acetate in the base media, as well as small amounts of sugars and/or amino acids
179 catabolized by *P. alactolyticus*. However, consumption of background media
180 components by *P. alactolyticus* was negligeable when acetate and lactate were
181 abundant as confirmed by carbon balances (Supplementary Material Fig. 2),
182 indicating that acetate and lactate were the primary substrates for RBO. Interestingly,
183 *A. caccae* growth and lactate consumption was higher on base media compared to
184 media supplemented with 100 mM lactate and 0 to 8 mM (low) acetate (Fig. 2c,
185 Supplementary Material), highlighting this organism's requirement for acetate as a
186 co-substrate to lactate. To confirm that background media components had minimal
187 effects on the results of our study, experiments were reproduced in dilute media,
188 showing identical trends (Supplementary Material Fig. 3 a,c,e).

189

190 **Favouring acetate recycling allows *P. alactolyticus* to maintain growth under**
191 **acetate scarcity**

192

193 Acetate recycling through PTA and ACK could allow *P. alactolyticus* to consume less
194 acetate than *A. caccae*, thereby reducing its reliance on it as a co-substrate. To evaluate
195 whether acetate recycling is more prevalent in *P. alactolyticus*, we compared acetate
196 consumption by both organisms across acetate-to-lactate ratios to its expected value
197 if no acetate were recycled. Without recycling, one mole of acetate is consumed for
198 each mole of product formed, so expected acetate consumption is the molar sum of
199 products formed. With *A. caccae*, acetate consumption was slightly inferior to its
200 expected value for all tested ratios, suggesting minimal recycling (Fig. 3a). On the
201 other hand, acetate consumption by *P. alactolyticus* was significantly lower than
202 expected if one mole of acetate was assimilated for each mole of product. In fact,
203 minimal production was detected at low ratios (Fig. 3a), indicating that acetate
204 recycling by *P. alactolyticus* is superior to that by *A. caccae*.

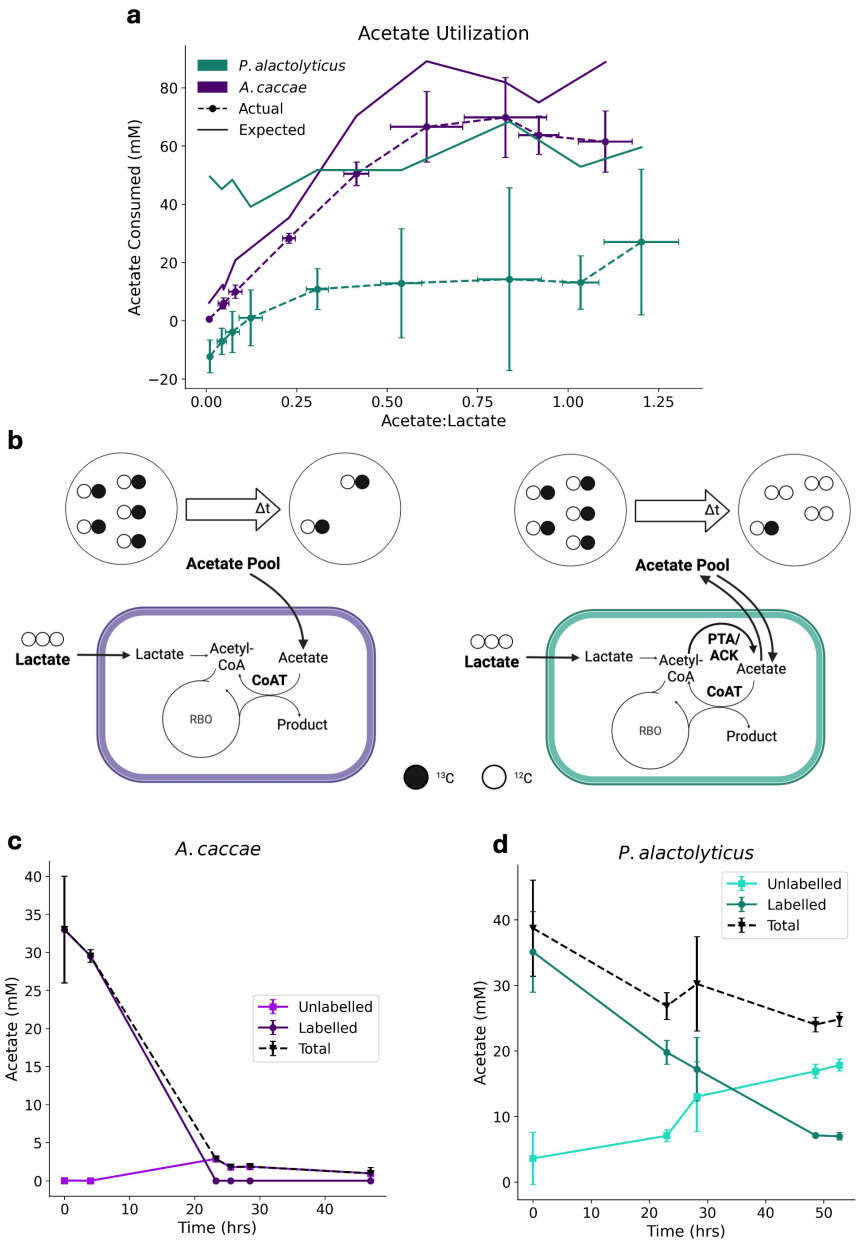

Figure 3. 1-^{13}C acetate tracing shows different acetate utilization strategies in *A. caccae* and *P. alactolyticus*. a. Measured acetate consumption and consumption expected if no recycling were occurring at different acetate-to-lactate ratios (n=3). **b.** Left: Schematics of full acetate assimilation in the tracing experiment. Recycling is minimal and acetate pool labelling pattern does not significantly change after a period of time (Dt). Acetate pool concentration decreases due to assimilation, via CoAT. ^{13}C Labeled carbon presented as a black circle. Right: Schematics of a highly active acetate recycling, through acetate regeneration via PTA/ACK. Acetate labelling pattern drastically changes over time, with limited assimilation.

215 Biorender.com/coz8d26. **c.** 1-^{13}C-acetate tracing throughout batch growth of *P. alactolyticus.* **d.**
216 and *A. caccae* (n=3). *P. alactolyticus* recycles acetate readily, causing low net consumption,
217 whereas recycling in *A. caccae* is minimal.
218
219 To confirm this, we performed a tracing experiment by supplementing 1-^{13}C labeled
220 acetate to *A. caccae* and *P. alactolyticus* during lactate fermentation (Fig. 3b). In this
221 experiment, we anticipated two possible outcomes. In the first, consumed acetate
222 would be assimilated into carboxylic acids, with any remaining acetate being labeled.
223 This would be indicative of minimal to no recycling. In the second, labeled acetate
224 would be incorporated into carboxylic acids while unlabeled acetate would be
225 produced via unlabeled lactate oxidation and PTA/ACK reactions. Then, labeled
226 acetyl-CoA pool would be substantially diluted, resulting in an extracellular acetate
227 pool containing both unlabeled and labeled acetate. This would indicate strong
228 acetate recycling. The first scenario was observed in *A. caccae* (Fig. 3c), where labeled
229 acetate was depleted and an insignificant amount of unlabeled acetate was generated,
230 indicating minimal but detectable recycling. We observed the second scenario in *P.*
231 *alactolyticus* (Fig. 3d), where most of the 1-^{13}C-acetate was assimilated and the major
232 fraction of the extracellular acetate pool was unlabeled. A similar result has been
233 obtained with *C. kluyveri* using labeled ethanol and acetate[37]. These results support
234 that *P. alactolyticus*, unlike *A. caccae*, does not depend strongly on acetate as a co-
235 substrate because acetate is readily recycled through PTA/ACK, reducing net
236 consumption requirements.
237
238 **Favouring acetate recycling requires long chain products for redox balance and**
239 **reduces chemiosmosis**
240
241 We then asked whether either organism's bias towards acetate assimilation or
242 recycling shifted across acetate-to-lactate ratios. Also, it remained unclear why *A.*
243 *caccae* was incapable of strongly recycling acetate, and how acetate utilization affected
244 product spectra and energy conservation. To address these questions, we used a
245 stoichiometric model of RBO (Fig. 4a, Stoichiometric Model in Methods) to quantify

moles of acetate recycled per mole of product (θ). This established that an increase in RBO cycles (n) is required to recycle acetate strongly ($\theta > 0.5$). Model fluxes were calculated based on substrate consumption and product formation measurements across a wide range of acetate-to-lactate ratios (0.08 – 1.2 mol/mol in base ATCC 2107 media, Fig. 2b,e, Fig. 3a; 0.02-1 mol/mol in dilute ATCC2107 media, Supplementary Material Fig. 4).

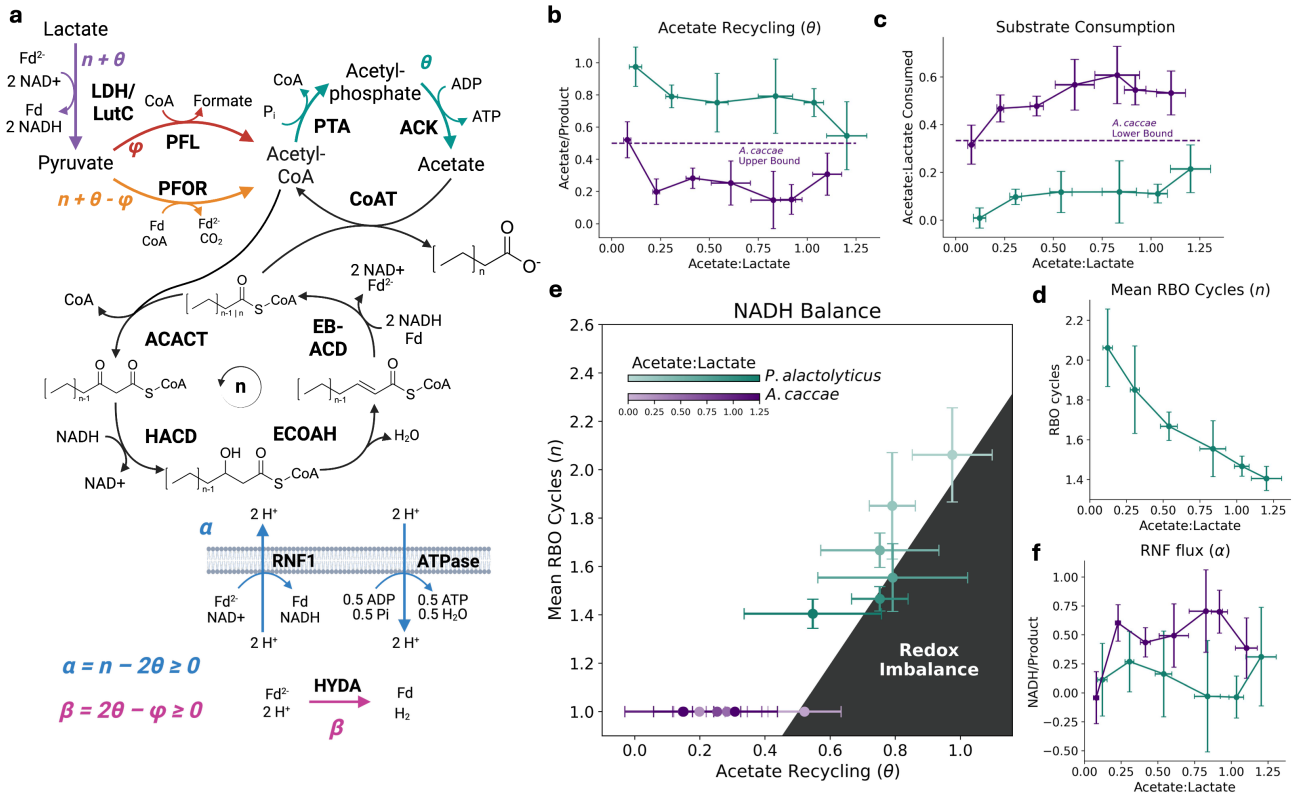

Figure 4. Stronger recycling requires more RBO cycles on average and reduces chemiosmosis. **a.** Stoichiometric model of RBO with simultaneous acetate assimilation and recycling, where θ is the extent of acetate recycling (moles recycled per mole product) and n is the mean number of RBO cycles. LDH = electron bifurcating lactate dehydrogenase; LutC = lactate utilization protein C; PFOR = pyruvate:ferredoxin oxidoreductase; PFL = pyruvate formate lyase; PTA = phosphate acetyltransferase; ACK = acetate kinase; ACACT = acetyl-CoA C-acetyltransferase; HACD = 3-hydroxyacyl-CoA dehydrogenase; ECOAH = enoyl-CoA hydratase; EB-ACD = electron bifurcating acyl-CoA dehydrogenase, comprising acyl-CoA dehydrogenase (ACD) and electron transfer flavoproteins A and B (EtfA and EtfB); CoAT = acyl-CoA:acetate CoA transferase; Fd = ferredoxin; RNF1 = proton translocating ferredoxin: NAD+ oxidoreductase complex; ATPase:

264 F0/F1 ATP synthase; HYDA = Fe–Fe hydrogenase. BioRender.com/r3otw9j. **b.** Acetate recycling
265 as a function of acetate-to-lactate ratio for *P. alactolyticus* and *A.* caccae. **c.** Ratio of acetate-to-
266 lactate consumption by *P. alactolyticus* and *A. caccae* across ratios of supplemented acetate and
267 lactate. **d.** Mean number of RBO cycles (n) in *P. alactolyticus* as a function of acetate-to-lactate
268 ratio. **e.** Experimentally derived pairs of n and θ, and inequality relating these parameters for
269 maintenance of redox balance ($\alpha > 0$). When acetate is scarce, production of longer-chain
270 products by *P. alactolyticus* enables strong acetate recycling ($\theta > 0.5$) by balancing the reduction
271 equivalents released by increased lactate oxidation, thereby maintaining null or positive flux
272 through RNF. Since *A. caccae* only produces butyrate, redox balance is not possible for $\theta > 0.5$,
273 meaning acetate and lactate must be consumed in a ratio of at least 1/3. **f.** Flux through RNF
274 relative to product flux (α).
275
276 When acetate was plentiful, acetate recycling by *A. caccae* was minimal ($\theta \approx 0.2$). In
277 this case, NADH produced from lactate is inferior to NADH consumed by the single
278 RBO cycle which synthesizes butyrate ($n = 1$). The reduced ferredoxin produced by
279 electron bifurcation in RBO drives the RNF complex to regenerate and balance
280 NADH. Acetate recycling by *A. caccae* increased when less acetate was supplemented
281 (Fig. 4b). This facilitated lactate utilization, since acetate recycling reduces the ratio in
282 which acetate and lactate are consumed (Fig. 4c). When 0.5 moles of acetate are
283 recycled for each mole of butyrate produced ($\theta = 0.5$), NADH production from lactate
284 matches consumption by RBO and RNF flux goes to 0. Assuming that reverse flux
285 through RNF is infeasible, we hypothesized that *A. caccae* could not achieve $\theta > 0.5$
286 because NADH would accumulate. This means *A. caccae* would need to consume
287 acetate and lactate in a ratio of at least 1/3. Indeed, θ was smaller or equal to 0.5 and
288 α was larger or equal to 0 in all conditions, and the ratio of acetate-to-lactate
289 consumption did not fall significantly below 1/3. This lower bound explains why
290 growth and lactate utilization by *A. caccae* dropped sharply between acetate-to-lactate
291 supplementation ratios of 0.5 and 0.25 (Fig. 2c,d).
292
293 On the other hand, *P. alactolyticus* maintained growth and full lactate utilization when
294 acetate was scarce. As suggested previously, this is due to its enhanced capacity for

295 acetate recycling: *P. alactolyticus* achieved $\theta \geq 0.5$ in all tested conditions, with full
296 recycling ($\theta \approx 1$) occurring at low acetate-to-lactate ratios. This was impossible in *A.*
297 *caccae* as NADH from lactate oxidation would quickly accumulate, but unlike *A.*
298 *caccae*, *P. alactolyticus* can produce hexanoate and octanoate in addition to butyrate.
299 As these MCCAs require more NADH, stronger acetate recycling is possible without
300 the loss of redox balance. Indeed, *P. alactolyticus* favoured MCCA production as
301 acetate supplementation was reduced and θ approached 1 (Fig. 4b,d,e). Heightened
302 NADH production from lactate was counteracted by increasingly lengthened
303 products (increasing n) and predicted RNF flux remained within a 95% CI of 0 (Fig.
304 4f). Thus, we propose that by favouring MCCA production when acetate is scarce, *P.*
305 *alactolyticus* can fully recycle acetate while maintaining redox balance. This explains
306 why, unlike *A. caccae*, *P. alactolyticus* does not require acetate as a co-substrate and
307 maintains full lactate utilization when acetate is scarce. Increased acetate recycling
308 accompanied by an increase in product chain length was also observed in two other
309 CEB, *Clostridium kluyveri* and *Megasphaera hexanoica*, when we grew them in diluted
310 ATCC 2107 medium (Supplementary Material Fig. 4). Interestingly, *C. kluyveri*
311 recycled acetate less than *P. alactolyticus* in acetate limited conditions (θ of 0.60 and
312 1.21, respectively) (Supplementary Material Fig. 4b, Supplementary Material S1). *C.*
313 *kluyveri* also ran fewer RBO cycles than *P. alactolyticus* (n of 1.82 and 2.26, respectively)
314 (Supplementary Material Fig. 4d, Supplementary Material S1), resulting in
315 negligeable octanoate production. This is consistent with previous findings with *C.*
316 *kluyveri*[38,39]. On the other hand, *M. hexanoica*, like *P. alactolyticus*, favoured octanoate
317 production as acetate recycling increased (Supplementary Material Fig. 3f). These
318 results indicate that octanoate production enhances capacity for acetate recycling.
319
320 Acetate recycling may also increase hydrogen production (Supplementary Material
321 Fig. 5). As was established, acetate recycling enables more lactate utilization when
322 acetate is limiting. Stoichiometrically, this releases more NADH, reducing flux
323 through the RNF complex via product inhibition. The resulting accumulation of
324 reduced ferredoxin can be balanced with hydrogen production by HYDA flux (β).

325 Alternatively, reduced ferredoxin production can be tempered by redirecting
326 pyruvate from PFOR to PFL: when forming acetyl-CoA, PFOR reduces ferredoxin and
327 produces CO_2, whereas PFL only produces formate. The puzzling redundancy of PFL
328 and PFOR may then be functional. Flux through PFL (φ) allows for some electrons to
329 be balanced with formate rather than hydrogen when acetate is recycled, potentially
330 preventing rapid accumulation of H_2. Heightened hydrogen partial pressure has been
331 shown to hinder chain elongation due to thermodynamic constraints[40]. Notably, if flux
332 through HYDA must be positive or null, formate production requires some acetate
333 recycling. Otherwise, there would not be enough reduced ferredoxin to regenerate
334 NADH for RBO through RNF. Indeed, formate measurements from select acetate-to-
335 lactate ratios predict non-negative HYDA flux for both organisms (Supplementary
336 Material Fig. 6). PFL flux is higher in *P. alactolyticus* than *A. caccae*, particularly at low
337 acetate-to-lactate ratios when acetate recycling is more prevalent and more ferredoxin
338 must be balanced.
339
340 It has been reported that in other chain elongators such as *C. kluyveri,* the HACD
341 enzyme in RBO can use NADPH instead of NADH to reduce oxoacyl-CoAs. Here, the
342 NFN complex would regenerate NADPH from NADH and reduced ferredoxin
343 through electron confurcation[22,41]. This would increase the number of RBO cycles
344 required for acetate recycling, since less NADH is balanced by each RBO cycle (see
345 stoichiometric model in *Methods*). Our data suggests that NFN does not play a major
346 role in RBO for *P. alactolyticus* and *A. caccae*, since these organisms satisfy the redox
347 constraint predicted when NFN flux is negligeable (Supplementary Material Fig. 7 for
348 further discussion). However, NFN was found in both proteomes (Supplementary
349 Material S1) and likely plays a role in generating NADPH for anabolism.
350
351 Acetate recycling also has important implications for energy conservation in RBO.
352 Chemiosmosis is often assumed to be the primary mode of energy conservation in
353 CEB, with SLP playing a minor and static role. These results show that SLP becomes
354 increasingly prevalent in both *A. caccae* and *P. alactolyticus* as acetate supplementation
355 is reduced. Notably, stoichiometric analysis suggests that acetate recycling reduces

RNF flux and ATP yield on lactate (see Stoichiometric Model in Methods), with predicted RNF flux and ATP yield being lower at low acetate to lactate ratios for both *P. alactolyticus* and *A. caccae* (Fig. 1f, Supplementary Text). Taken together, these results suggest that acetate recycling imposes an ATP yield penalty and can require MCCA production (for $\theta > 0.5$). Under acetate limitation, increased lactate utilization enabled by recycling may outweigh these potential drawbacks.

Acetate recycling and requisite production of longer chain products impose higher metabolic burden, reducing growth rate

In addition to energy yield, a critical characteristic of a metabolic strategy is enzyme cost[42–44]. Each reaction in a metabolic pathway demands the synthesis and maintenance of an enzyme pool. Given an arbitrary pathway flux, the size of this pool is a function of the enzyme's saturation and the reaction's thermodynamic driving force. It follows that a longer pathway and/or a pathway with more reactions near equilibrium will require more enzyme per unit flux. Resource allocation arguments suggest that a higher catabolic enzyme cost per ATP flux is likely to slow growth, since fewer resources (i.e., biomass) are free to engage in anabolism[8].

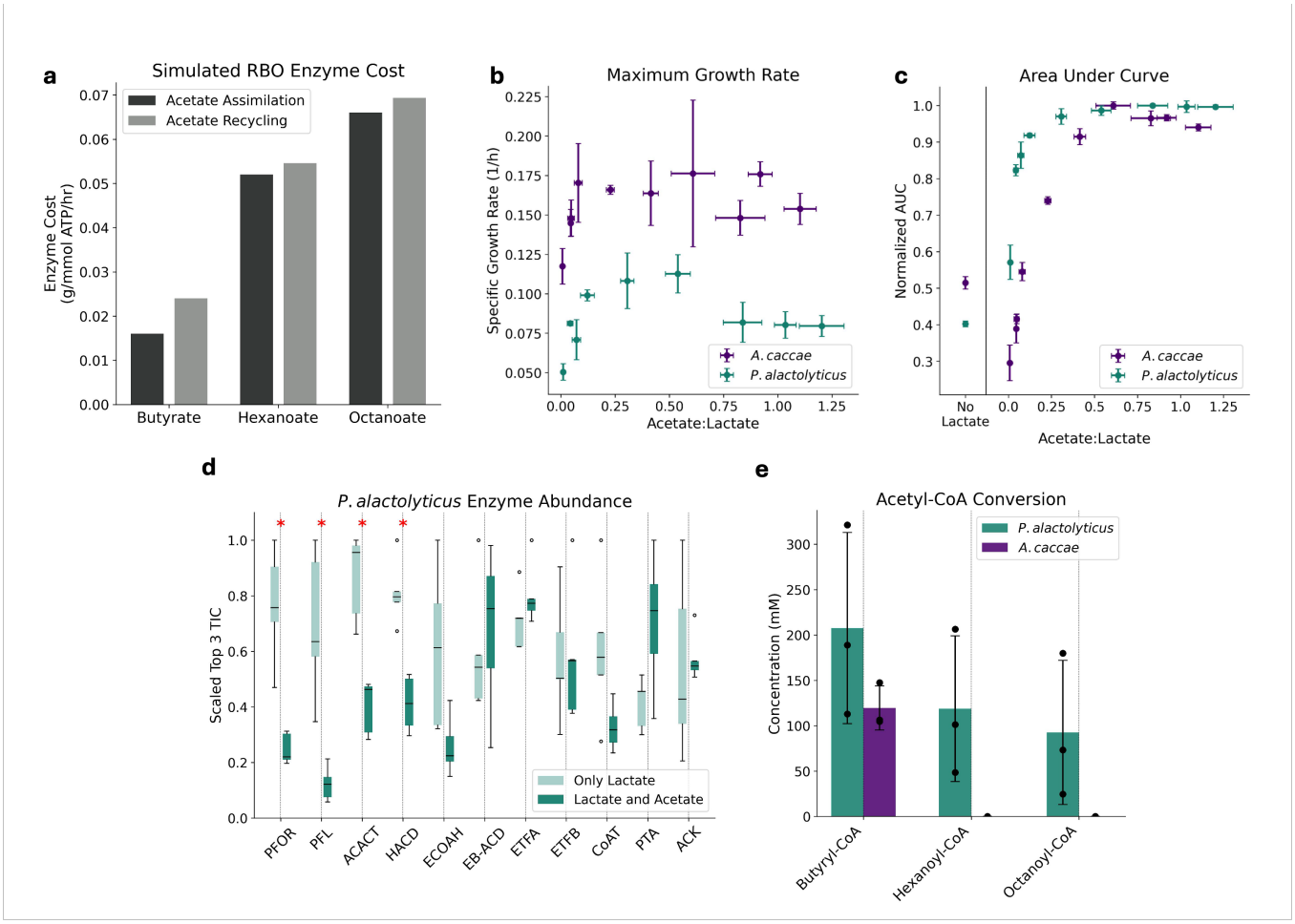

Figure 5. Trade-off between efficient acetate utilization and metabolic burden/growth rate and the restriction of *A. caccae*'s CoAT to acyl-CoA beyond C4. a. Predicted enzyme cost per unit ATP flux (g/mmol ATP/hr) required to produce butyrate, hexanoate and octanoate with and without acetate recycling **b.** Maximum growth rates achieved by *P. alactolyticus* and *A. caccae* at different acetate-to-lactate ratios. **c.** Area under the growth curves for *P. alactolyticus* and *A. caccae* **d.** Differential proteomics on *P. alactolyticus* grown on lactate with and without acetate (n=5). Top 3 Total Ion Current (Top 3 TIC) was used as comparison metrics. Each data point was scaled by the maximum value of the corresponding enzyme across all conditions.* $p < 0.05$. **e.** Acyl-CoA CoA transfer reaction using *A. caccae*'s and *P. alactolyticus*' cell lysate. All replicates are biological. Recycling acetate and/or producing longer products requires a larger pool of RBO enzymes, likely contributing to the growth rate penalty assumed by *P. alactolyticus* as compared to *A. caccae* and by both organisms when acetate-to-lactate ratio is reduced. *P. alactolyticus*' CoAT reacts with C4-C8 acyl-CoAs, while *A. caccae*'s is limited to C4.

390 Enzyme Cost Minimization (ECM)[43] was used to approximate a lower bound for RBO
391 enzyme cost per ATP flux for butyrate, hexanoate or octanoate production with full
392 acetate recycling or full assimilation. ECM predicted that thiolase (ACACT) reactions
393 are the main thermodynamic bottleneck in RBO (Supplementary Material Fig. 8). At
394 the total enzyme cost minimum, the effects of this bottleneck are spread across other
395 reactions, including HACD, ECOAH and EB-ACD, increasing their enzyme cost.
396 Thiolase reactions are increasingly unfavourable as chain length grows
397 (Supplementary Material Fig. 8), therefore MCCA production engenders a higher
398 total enzyme cost than butyrate production. Acetate recycling further heightens
399 enzyme cost due to PTA and ACK and reduced ATP yield on lactate (Fig. 5a,
400 Supplementary Material Fig. 9). Therefore, acetate recycling likely imposes a growth
401 rate penalty, particularly if MCCAs are produced to strongly recycle acetate ($\theta > 0.5$).
402 This is consistent with the faster specific growth rates of *A. caccae* vs. *P. alactolyticus*
403 measured from batch cultures with different acetate to lactate ratios (Fig. 2b,c, Fig.
404 5b): *A. caccae* minimizes enzyme cost by favouring acetate assimilation and only
405 producing butyrate, while *P. alactolyticus* assumes the higher enzymatic burden
406 required produce MCCAs, enabling strong acetate recycling. This allows *P.*
407 *alactolyticus* to maintain growth and lactate consumption when acetate is scarce (Fig.
408 5c, Fig. 2d).
409
410 Since ECM predicts enzyme cost per unit flux, a higher cost could be reflected in both
411 heightened protein expression and/or reduced flux. To test whether favouring acetate
412 recycling and MCCA production is facilitated by changes in protein expression, we
413 performed differential proteomics analysis on *P. alactolyticus* (Fig. 5d) with and
414 without acetate supplementation. We observed increased expression in PFOR and
415 PFL when acetate was not provided. This may facilitate more pyruvate flux to acetyl-
416 CoA, compensating for increased diversion of acetyl-CoA to acetate recycling.
417 Additionally, we observed heightened expression of ACACT and HACD when
418 acetate was not supplemented and MCCA production was favoured, consistent with
419 ACACT reactions being more thermodynamically constrained for MCCAs. While
420 ECM suggested that MCCA production imparts higher demand for ECOAH and

421 EBACD, expression of these enzymes did not change significantly. This discrepancy
422 is not unexpected, since ECM finds an optimal distribution of metabolite
423 concentrations that may not reflect intracellular conditions. These enzymes may also
424 be more catalytically efficient than expected. Similarly, expression of CoAT, PTA and
425 ACK did not change significantly. Nonetheless, these results support that favouring
426 MCCA production when acetate is scarce imposes an enzyme cost penalty and
427 involves gene expression control in *P. alactolyticus*.
428
429 ***A. caccae*'s CoAT activity is limited to butyryl-CoA, preventing further elongation**
430 **to MCCAs**
431
432 Despite the impact of acetate utilization strategies on product chain length, lactate
433 utilization, energy conservation, growth and gene expression, the molecular
434 mechanism that constrains *A. caccae*'s products to butyrate while enabling *P.*
435 *alactolyticus* to synthesize MCCAs remains unclear. One possible explanation could
436 be enzyme specificity. In the synthetic RBO in *E. coli*, thioesterases are employed to
437 terminate elongation cycles by acting on CoA/ACP intermediates, and they are
438 crucial for controlling carboxylic acid chain length[9,45,46]. Analogously, CoA
439 transferases terminate elongation cycles in CEB and may have a similar role in
440 specifying chain length. Some CoATs have been heterologously expressed and
441 characterized in *E. coli,* where it was observed that CoATs from butyrate-producing
442 CEB have preference for butyryl-CoA and no activity on hexanoyl-CoA[47–49].
443
444 To investigate CoAT specificity in *A. caccae* and *P. alactolyticus*, we obtained cell
445 lysates from both organisms and provided acetate and butyryl-CoA, hexanoyl-CoA
446 or octanoyl-CoA as substrates. With *A. caccae*'s lysate, activity was observed on
447 butyryl-CoA but not hexanoyl-CoA. *P. alactolyticus* lysate, on the other hand,
448 exhibited activity not only on butyryl-CoA but also hexanoyl-CoA and octanoyl-CoA
449 (Fig. 5e). Notably, our proteomics data indicate that a single allele is responsible for
450 CoAT activity in both *A. caccae* and *P. alactolyticus*, although multiple CoAT and
451 thioesterase genes are encoded by both organisms. Nonetheless, these results suggest

452 that CoAT specificity is strict in *A. caccae* and broader in *P. alactolyticus*, and providing
453 the first report of CoAT activity on octanoyl-CoA.
454

455 # Discussion

456 While the role of acetate in CEB was debated in the decades following their discovery
457 in 1939[10,18,37,40,50–52], the consensus has since become that acetate is mainly assimilated,
458 with IMF being the primary mode of energy conservation. Our results challenge this
459 view, as we show that while the butyrate-producer *A. caccae* favours acetate
460 assimilation and energy conservation via IMF, *P. alactolyticus* favours acetate
461 recycling and SLP, producing MCCAs to balance additional redox equivalents from
462 increased lactate oxidation. As a result, *A. caccae* must consume acetate as a co-
463 substrate, whereas *P. alactolyticus* can grow and consume lactate without net acetate
464 consumption. While the present work has focused on lactate-based chain elongation,
465 the stoichiometry of redox equivalents for ethanol-based chain elongation is highly
466 analogous—in both cases, 2 moles of NADH are produced per mole of electron donor.
467 Consequently, ethanol-consuming CEB such as *C. kluyveri* also produce MCCAs to
468 recycle acetate when it is scarce, as evidenced by supplementary experiments
469 (Supplementary Material Fig. 4b-4d) and in previous open culture studies[53,54]. Specific
470 redox balances with other electron donors used by CEB (sugars[36,55], methanol[56,57],
471 propanol[58]) will vary. However, in all cases recycling acetate will increase electron
472 donor oxidation. Therefore, redox balance under acetate recycling is likely to require
473 synthesis of longer-chain, more reduced products.
474

475 We show that the specific CoAT enzyme variants encoded by CEB are critical for
476 controlling sole butyrate versus MCCA production. In *A. caccae*, CoAT is specific to
477 butyryl-CoA as has been previously shown for other CEB[47,48], whereas in *P.*
478 *alactolyticus* it acts on butyryl-CoA, hexanoyl-CoA and octanoyl-CoA (Fig. 5e). In
479 addition to CoAT, ACACTs (thiolases) from *M. hexanoica* and *C. kluyveri* have been
480 shown to enhance C6 production in *E. coli*, suggesting that these enzymes also present
481 chain-length specificity[59,60]. Conventional top-down microbiome engineering

482 approaches that rely on selection pressure and manipulation of bioprocess parameters
483 do not consider how these genetic differences constrain process performance. Using
484 CoAT gene sequences as biomarkers for MCCA-production potential could track
485 MCCA-producing CEB in bioreactors and improve inoculum selection. Moreover,
486 engineering these enzymes for greater control of MCCA chain length will be a key
487 molecular intervention to boost product selectivity.
488
489 Substrate specificity of CoAT helps explain why *P. alactolyticus* can synthesize
490 MCCAs and *A. caccae* cannot, affording the former enhanced capacity for acetate
491 recycling and efficient lactate utilization. However, CoAT specificity does not explain
492 how acetate recycling is increased in response to acetate limitation. Favouring acetate
493 recycling may be a passive process, where the reduction of intracellular acetate
494 concentration during acetate limitation increases the thermodynamic driving force
495 and net flux through PTA and ACK compared to lactate oxidation. Likewise, CoAT
496 specificity in *P. alactolyticus* is likely not responsible for favouring MCCA production
497 when acetate is limiting, since proteomic data suggests that *P. alactolyticus* uses a
498 single CoAT for C4, C6 and C8 carbon intermediates (Fig. 5d). Instead, increased
499 MCCA production appears to involve gene regulation to modulate RBO enzyme
500 levels. Through differential proteomic analysis, we observed that ACACT and HACD
501 abundances increased significantly in *P. alactolyticus* when acetate was not
502 supplemented and MCCA production increased. This is consistent with ACACT
503 being the main thermodynamic bottleneck in RBO[61].
504
505 The mechanism for upregulating RBO enzyme expression likely involves the redox-
506 sensing transcriptional regulator Rex, which responds to changes in $NADH/NAD^+$
507 ratios. If acetate recycling increases passively in response to acetate limitation, there
508 would likely be a transient excess of NADH which triggers Rex. The Rex consensus
509 binding site[62,63] has been identified in the promoter regions of RBO enzyme genes,
510 including ACACT and HACD, in *C. kluyveri*[62], *Caproicibacterium lactatifermentans*[36] and
511 *Clostridium acetobutylicum*[63]. In *P. alactolyticus* genome, sequences nearly identical to
512 the consensus can be found upstream of the *acact-ecoah-hacd* operon and the *coat* gene

513 (Supplementary Material S1), suggesting that Rex has an important role in the
514 regulation of RBO genes. As ACACT (initiation) and CoAT (termination) compete for
515 the same substrate, the increase in ACACT and HACD highlighted in our differential
516 proteomics would favor elongation over termination, resulting in longer products.
517 Alternatively, acetylphosphate and acetyl-CoA could be involved in this regulation,
518 as their intracellular concentrations would decrease in response to lower acetate
519 availability. Acetylphosphate is a known signalling molecule in two-component
520 systems[64–66], while both acetylphosphate and acetyl-CoA participate in lysine
521 acetylation, a post-translational modification[67,68].
522
523 Aside from underlying regulatory mechanisms and enzymatic specificities, capacity
524 for acetate recycling may represent a fundamental ecological distinction between
525 butyrate-producing and MCCA-producing CEB. We suggest that, since butyrate
526 producing CEB cannot strongly recycle acetate, their growth and lactate consumption
527 is limited by acetate availability, as shown above with *A. caccae* (Fig. 1d). On the other
528 hand, MCCA producers are capable of strong acetate recycling. This allows them to
529 maintain lactate utilization when acetate is scarce, demonstrated here with *P.*
530 *alactolyticus* (Fig. 1d). As a result, MCCA-producing CEB may outcompete butyrate-
531 producing CEB when acetate concentration or feeding rate is low. When acetate is
532 abundant, butyrate production would likely outcompete MCCA production, since
533 butyrate production requires less enzyme investment and may therefore enable faster
534 growth. Accordingly, we propose that environments with low acetate-to-lactate ratios
535 select for MCCA producing CEB, whereas those with high acetate-to-lactate ratios
536 select for butyrate producing CEB.
537
538 The environments from which *P. alactolyticus* and *A. caccae* were isolated support this
539 hypothesis. *P. alactolyticus* was isolated from human infection sites[69] where lactate is
540 likely to be enriched, such as infections of the lungs[70], brain[71], and teeth[72]. Conversely,
541 *A. caccae* was isolated from the human gut where acetate accumulates to high
542 concentrations (>50 mM) and is the most abundant SCCA[73–76]. More generally, lower
543 acetate-to-electron donor supplementation ratios promoted MCCA production over

544 butyrate in open culture batch reactors, although propionate production appears to
545 have tempered MCCA production at very low ratios[34,77,78]. Lower ratios of acetate-to-
546 lactate feed rates favoured hexanoate production over butyrate in a continuously fed
547 open culture reactor[78], consistent with MCCA production enabling increased acetate
548 recycling for faster lactate utilization when acetate feed rate is limiting. Contrary to
549 our expectation, in a semi-continuous chain elongation reactor fed lactate and xylan
550 at constant rates without acetate, butyrate producers eventually outcompeted MCCA
551 producers. However, this shift was associated with the enrichment of potential acetate
552 producers (*Syntrophococcus*), which could have increased acetate cross-feeding and
553 given a competitive advantage to butyrate producers[79]. Overall, these bioprocess
554 studies support that acetate utilization strategy is a key ecological differentiator of
555 butyrate and MCCA-producing CEB, with the latter's capacity for acetate recycling
556 being advantageous when acetate is limiting.
557
558 Our findings point to key genetic, physiological and ecological determinants of
559 MCCA production, supporting new bioengineering and bioprocess developments.
560 Key limitations of conventional MCCA production with microbiomes are the lack of
561 control over microbial interactions and genetics, causing poor MCCA yield and
562 selectivity. Our work suggests that tailoring microbiome function to limit acetate
563 cross-feeding would favour MCCA production over butyrate. We also show that
564 CoAT enzymes from CEB have evolved different substrate preferences, which creates
565 an opportunity to rationally engineer CoAT to enhance control over MCCA chain
566 length. We anticipate that achieving these interventions could be accelerated by
567 bottom-up microbiome engineering[80], enabling more precise MCCA upcycling for a
568 sustainable bioeconomy.
569
570
571
572
573
574

575

576 # Methods

577 **Bacterial strains and culturing conditions**

578 *Pseudoramibacter alactolyticus* DSM 3980 and *Anaerostipes caccae* DSM 14662 were
579 purchased from the German Collection of Micro-organisms and Cell Cultures
580 (DSMZ). Both organisms were cultured in Modified Reinforced Clostridial Medium
581 (ATCC 2107) with minor modifications. Starch was removed and glucose was
582 replaced for lactic acid. Chemicals were purchased from BioShop (Burlington, ON,
583 Canada) unless otherwise stated. Beef extract, 10 g L^{-1}; Tryptose (Milipore,
584 Burlington, MA, USA), 10 g L^{-1}; NaCl, 5 g L^{-1}; yeast extract, 3 g L^{-1}; sodium acetate,
585 varied concentrations; lactic acid, varied concentrations; resazurin, 0.01% (Sigma-
586 Aldrich, St. Louis, MO, USA); L-cysteine.HCl, 0.5 gL^{-1}. pH was adjusted to 6.8. After
587 autoclaving, culture medium was purged with N_2/CO_2 gas mix (80%/20%). Batch
588 kinetics were conducted in media bottles sealed with rubber stoppers. Acetate-to-
589 lactate ratio experiment was conducted in 96-well plates. 1-^{13}C acetate tracing and cell
590 growth for proteomics were conducted in Hungate tubes. Both strains were statically
591 incubated at 37°C in all experiments.

592

593 **Lactate, formate and carboxylic acids quantification**

594 All samples were filtered through a 0.2 μm membrane and stored at −20 °C. Prior to
595 analysis, samples were thawed, centrifuged at 17,000 × g for 2 minutes, and diluted
596 appropriately with HPLC-grade water. Lactate and formate were quantified using
597 high-performance liquid chromatography (HPLC) on an UltiMate 3000 system
598 (Thermo Fisher Scientific, Waltham, MA, USA) equipped with an Aminex HPX-87H
599 column (300 × 7.8 mm, 9 μm, Bio-Rad, Hercules, CA, USA) and a compatible guard
600 column. The mobile phase consisted of 5 mM sulfuric acid, and elution was
601 performed at a flow rate of 0.6 mL/min. The column was maintained at 50 °C.
602 Ultraviolet (UV) detection was used for compound identification and quantification.
603 Data acquisition and analysis were carried out using Chromeleon 7 software
604 (Thermo).

605

606 Acetate, butyrate, hexanoate and octanoate were measured using gas
607 chromatography (8900 GC System, Agilent, Santa Clara, CA, USA) with tandem mass
608 spectrometry (7000D Triple Quadrupole GC-MS, Agilent) and DB-FatWax column
609 (Agilent). Carboxylic acids in the standards and diluted samples were protonated
610 with formic acid to a final concentration of 0.1 M. 0.3 μL of each sample were injected
611 with a split ratio of 10:1. The run time was 16 min and the temperature gradient as it
612 follows: 80°C for 1 minute, a 20°C/min ramp until 200°C, 5°C/min until 210°C,
613 20°C/min until 250°C and finally held for 5 mins. The carrier gas was helium at a flow
614 rate of 1 mL/min. The mass spectrometer was operated either in scan mode (96-well
615 batches and acetate tracing) or dynamic multiple reaction monitoring (dMRM) mode
616 (Batch kinetics). Target analytes were ionized and fragmented by electron ionization.
617 The precursor ion and product ion of target analytes (dMRM) were selected using
618 Agilent software (MassHunter Optimizer, Agilent). To quantify ^{13}C labeled acetate,
619 m/z 61 was used while m/z 60 was used for unlabelled acetate.

620

621 **Protein extraction and digestion**

622 Biomass was collected during mid-exponential phase by centrifugation, washed once
623 with Phosphate Buffered Saline (PBS), pH 7, and frozen with liquid N_2. Cell pellets
624 were stored at −80°C until further processing. Protein was extracted and digested as
625 described by Lawson et al.[81] ,with minor modifications. Cell pellets were resuspended
626 in 175 μL of 1% sodium deoxycholate in 50 mM triethylammonium bicarbonate
627 (TEAB) buffer, pH 8, and mixed 1:1 (v:v) with B-PER (Thermo Fisher). Cells were
628 lysed with 100 μm acid washed glass beads (Sigma) by vortexing at 2500 rpm for 1
629 minute. This process was repeated 4 more times with intermittent incubation on ice
630 for 30 seconds. Samples were then frozen at -80°C to aid the lysis process and slowly
631 thawed on ice. Once thawed, samples were vortexed for 1 minute and centrifuged at
632 14000 rpm for 10 minutes at 4°C. Protein quantification was carried out with Pierce™
633 Bradford Protein Assay Kit (Thermo Fisher). Cell lysate was then transferred to new
634 tubes and proteins were normalized by mass for differential proteomics. Next,

635 proteins were precipitated with trichloroacetic acid (TCA) at a final concentration of
636 20% and incubated on ice for 10 minutes. Samples were then centrifuged at 4°C and
637 14000 rpm for 5 minutes and protein pellet was washed twice with ice cold acetone.
638 Protein pellets were resuspended in 50 μL of 6M urea in 200 mM ammonium
639 bicarbonate (ABC) buffer. Next, dithiothreitol (DTT) in 200 mM ABC buffer was
640 added to a final concentration of 2.3 mM and samples were incubated at 37°C for 1
641 hour. Next, iodoacetamide (IAM) in 200 mM ABC was added to a final concentration
642 of 3.75 mM and samples were incubated at room temperature, in the dark, for 30
643 minutes. Prior to tryptic digest, samples were diluted with 200 mM ABC to reach a
644 urea concentration below 1M. Sequencing-grade trypsin (Promega, Madison, WI,
645 USA), 1:50 ratio trypsin to protein, was then added and samples were incubated
646 overnight at 37°C and 350 rpm. Peptide purification was carried out with OMIX Tips
647 (Agilent). Trifluoroacetic acid was added to the samples to a final concentration of 1%.
648 Next, OMIX C18 Tip was wet twice with 100 μL of a 1:1 mixture of acetonitrile (ACN)
649 and H_2O. Tip was equilibrated twice with 100 μL of 0.1% TFA and samples were
650 aspirated and dispensed 3-5 times. Next, tip was washed twice with 100 μL of 0.1%
651 TFA. Samples were eluted by aspiring and dispensing 100 μL of 95% ACN/0.1%
652 formic acid. Finally, samples were dried in speedvac and resuspended in 100 μL of
653 0.1% formic acid and filtered with 0.2 μm prior to injection.
654

655 **LC/MS parameters for peptide separation and detection**

656 All peptide samples were analyzed using a one-dimensional nano-flow LC-MS/MS
657 setup. Briefly, 10 μL of each sample was injected into an EASY-nano LC 1000 system
658 coupled to a Q-Exactive Orbitrap mass spectrometer (Thermo Scientific) via a nano-
659 electrospray ionization (nanoESI) source. Peptides were separated on a custom-
660 packed SilicaTip emitter column (New Objective, Woburn, USA) using ReproSil-Pur
661 C18-AQ resin (Dr. Maisch GmbH, Ammerbuch-Entringen, Baden-Württemberg,
662 Germany). The mobile phases consisted of solvent A (0.1% formic acid in H_2O) and
663 solvent B (0.1% formic acid in acetonitrile), and separation was achieved at a constant

flow rate of 250 nL/min. A gradient was applied as follows: 0 to 5 min 0% B, increase to 10% B; 5 to 93 min, increase to 40% B; 93 to 95 min, ramp to 95% B; held at 95% B until 105 min; returned to 0% B by 106 min and held until 120 min for column re-equilibration. The mass spectrometer operated in positive ion mode with a spray voltage of 3 kV and a capillary temperature of 275 °C. Full MS scans were acquired from 400 to 2,000 m/z at a resolution of 70,000, with an AGC target of 1e6 and a maximum injection time of 30 ms. For MS/MS acquisition, a Top10 data-dependent method was employed, isolating the top 10 most intense precursor ions within a 0.4 m/z isolation window. MS2 scans were acquired from 200 to 2,000 m/z at a resolution of 17,500, with a maximum injection time of 50 ms and a normalized collision energy (NCE) of 27.

Raw mass spectra data processing

Tandem mass spectra were extracted and converted to peak lists using the Global Proteome Machine (GPM; thegpm.org) pipeline (version 2020.11.12.1). Charge state deconvolution and deisotoping were not performed. MS/MS spectra were searched using X! Tandem (version X! Tandem Aspartate 2020.11.12.1) against custom protein databases for *P. alactolyticus* (NCBI TaxID: 113287) and *A. caccae* (NCBI TaxID: 105841), containing 2,285 and 3,294 protein entries, respectively. Protein FASTA files were obtained from the NCBI RefSeq database using genome assemblies ASM18550v1 (downloaded in February 2023) and ASM2018143v1 (downloaded in November 2023). Database searches were performed using trypsin as the digestion enzyme, with a precursor ion mass tolerance of 20 ppm and a fragment ion mass tolerance of 0.40 Da. Carbamidomethylation of cysteine and selenocysteine residues was specified as a fixed modification. Variable modifications included N-terminal pyro-glutamate formation from glutamine and glutamic acid, N-terminal ammonia-loss, deamidation of asparagine and glutamine, and oxidation or dioxidation of methionine and tryptophan residues.

693 Scaffold (version Scaffold_5.1.2, Proteome Software Inc., Portland, OR) was used to
694 validate MS/MS based peptide and protein identifications. Peptide identifications
695 were accepted if they could be established at greater than 95.0% probability by the
696 Peptide Prophet algorithm[82] with Scaffold delta-mass correction. Protein
697 identifications were accepted if they could be established at greater than 99.0%
698 probability and contained at least 2 identified peptides. Protein probabilities were
699 assigned by the Protein Prophet algorithm[83]. Proteins that contained similar peptides
700 and could not be differentiated based on MS/MS analysis alone were grouped to
701 satisfy the principles of parsimony. Up or downregulation of proteins were assessed
702 using Top 3 total ion current (TIC) as quantitative metric. The t-test was corrected
703 with Benjamini-Hochberg method.
704
705 **Cell lysate colorimetric assay**
706 *P. alactolyticus*' and *A. caccae*'s cell pellets were collected at mid exponential phase,
707 normalized by OD600 (0.8), washed once with 1x PBS, pH7 and stored at -80°C until
708 further processing. 10 mM Tris-HCl buffer (pH 7.5) containing 1 mM DTT and 40
709 mg/ml of lysozyme were added and samples were incubated at 37 °C for 20 minutes.
710 Next, 0.1g of 100 μm acid washed glass beads (Sigma) were added to aid cell lysis and
711 samples were vortexed at 2500 rpm for 1 minute, followed by ice incubation for 30
712 seconds. Vortex and ice incubation cycles were repeated 5 more times. Lysate was
713 centrifuged at 13500 rpm for 30 minutes at 4°C and clarified lysate was ultrafiltrated
714 with a 30 kDa MWCO concentrator for 30 minutes at 4°C. CoAT assay was coupled
715 to citrate synthase assay to detect free CoA, as described by Sato et al.[84], with minor
716 modifications. Briefly, 26 μL of lysate was combined with 10 μL of 40 mM phosphate
717 buffer, pH 7.4, 2 μL of 10 mM acyl-CoA (Sigma) and 2 μL of 2M sodium acetate.
718 Samples were incubated at 25°C for 5 min. Next, 40 μL of 8 mM oxaloacetic acid, 8
719 mM of 5,5′-dithiobis-2-nitrobenzoic acid (DTNB) and 46.5 μg/mL of citrate synthase
720 (NZYTech, Lisbon, Portugal) in 400mM phosphate buffer, pH 8, was added to each
721 assay. Samples were incubated at 37°C for 30 min. Absorbance was read at 412 nm
722 and negative controls for each condition did not have sodium acetate added. Acetyl-

723 CoA formation quantification was evaluated using acetyl-CoA (Sigma) to prepare a
724 calibration curve.
725
726 **Enzyme Cost Minimization (ECM)**
727 Python packages equilibrator-api and equilibrator-pathway
728 (https://gitlab.com/equilibrator) were used to perform ECM, developed by
729 Flamholz *et al*[43]. A reaction's enzyme demand $[E]$ (molar) given flux J is:
730

731 $$[E] = \frac{J}{k_{cat}} \frac{1 + \prod_i \left(\frac{K_{M,i}}{[C_i]}\right)^{m_i}}{1 - e^{\frac{\Delta G'}{RT}}}$$

732
733 k_{cat} is the forward rate constant, $[C_i]$ is the concentration of reactant i, $K_{M,i}$ is the
734 enzyme's saturation constant for reactant i, m_i is the stoichiometric coefficient of
735 reactant i, and $\Delta G'$ is the Gibbs free energy change, estimated via component
736 contribution at pH 6[85]. Total enzyme cost of a pathway per unit flux is minimized:
737

738 $$Minimize\ \Lambda = \frac{1}{J} \sum_i M_i\, n_i [E_i]$$

739 $$Such\ that\ C_{j,min} < C_j < C_{j,max}\ \forall j$$

740 $$And\ \Delta G'_i = \Delta G^{\circ\prime}{}_i + RT\boldsymbol{S}_i^T \cdot \ln(\boldsymbol{C}) < 0\ \forall i$$

741
742 Where $\boldsymbol{S}$ is the pathway's stoichiometric matrix and $\boldsymbol{C}$ contains metabolite
743 concentrations. For the ith reaction, n_i is its relative flux, M_i is its enzyme's molar
744 weight. Rate constants and saturation constants are shared across all enzymes (k_{cat} =
745 200 s^{-1}; K_m = 0.2 μM), molecular weights (MW) were taken from Uniprot
746 (https://www.uniprot.org/). Lower and upper bounds of pathway specific
747 metabolites are 1 μM and 10 mM, apart from oxoacyl-CoAs (lower bound of 0.4 μM
748 and upper bound of 10 mM). Universal metabolite (e.g. ATP) concentrations are
749 derived from literature[86]. The reduction potential of ferredoxin is set to -400 mV and

750 NADH to -280 mV. Saturation effects of redox equivalents are omitted. RNF, HYDA
751 and ATP synthase were not included in enzyme cost estimates.
752
753 **Stoichiometric Model**
754 n is the mean number of RBO cycles, derived from measurements of butyrate ($[B]$),
755 hexanoate ($[H]$) and octanoate ($[O]$) production:
756

757 $$n = \frac{[B] + 2[H] + 3[O]}{[B] + [H] + [O]}.$$

758
759 θ is the SLP flux per product flux (specific flux); $\theta = 0$ corresponds to complete
760 acetate assimilation and $\theta = 1$ to complete recycling. Molar product yield on acetate
761 ($Y_{Prod./Ac.}$) is related to acetate recycling through:
762

763 $$Y_{Prod./Ac.} = \frac{1}{1 - \theta}.$$

764
765 θ can therefore be estimated from butyrate, hexanoate and octanoate production and
766 acetate consumption data.
767

768 $$\theta = 1 - \frac{Acetate\ Consumed\ (mM)}{Products\ Formed\ (mM)}$$

769
770 Specific lactate consumption flux is $n + \theta$: increased acetate recycling requires that
771 more lactate is oxidized to supplement acetyl-CoA lost to SLP. Specific RNF flux, α,
772 is the difference of NADH production via lactate oxidation to acetyl-CoA and NADH
773 consumption by RBO cycles per mole of product. Since reverse flux through RNF is
774 predicted to be infeasible:
775

776 $$\alpha = -2(n + \theta) + 3n,$$

$$\alpha = n - 2\theta \geq 0\,.$$

Values of n and θ that satisfy this inequality correspond to combinations of product profile and acetate utilization strategy for which NADH balances; if the inequality is violated, redox balance would require negative flux through RNF to balance a surplus of NADH.

If a fraction of RBO cycles (ε) use an NADPH-dependent HACD and NFN to regenerate NADPH from NADH and reduced ferredoxin via electron confurcation, specific NFN flux equals $n\varepsilon$ and specific RNF flux becomes:

$$\alpha = -2(n + \theta) + 2n + n(1 - \varepsilon) + 0.5n\varepsilon$$
$$\alpha = n(1 - 0.5\varepsilon) - 2\theta$$

This reduces to the previous expression when $\varepsilon = 0$.

Specific HYDA flux is equal to ferredoxin reduced by EB-ACD minus ferredoxin oxidized by RNF and NFN, and ferredoxin diverted by PFL per mole of product:

$$\beta = n - \alpha - 0.5n\varepsilon - \varphi,$$
$$\beta = 2\theta - \varphi \geq 0\,.$$

ATP yield per mole of lactate is one half RNF flux plus SLP flux per lactate flux:

$$Y_{ATP/Lac.} = \frac{0.5\alpha + \theta}{n + \theta},$$
$$Y_{ATP/Lac.} = \frac{1}{2}\left(\frac{n(1 - 0.5\varepsilon)}{n + \theta}\right).$$

And if NFN flux is negligeable:

$$Y_{ATP/Lac.} = \frac{1}{2}\left(\frac{n}{n+\theta}\right)$$

See Supplementary Material S1 for calculations.

Data availability

The mass spectrometry proteomics data have been deposited to the ProteomeXchange Consortium via the PRIDE[87] partner repository with the dataset identifier PXD063079 and 10.6019/PXD063079. ECM models and python functions are available on GitHub (https://github.com/Connor-Bowers/Acetate-Utilization-Strategy).

Acknowledgements

The authors would like to acknowledge Joel Howard, Jasmeen Parmar and Diana Dyussekenova for the support on equipment operation. This work was supported by the Natural Sciences and Engineering Research Council of Canada [ALLRP 580897-22, RGPIN-2021-02684, NSERC-CREATE 528163-2019].

Conflict of Interest

The authors declare no conflicts of interest.

References

1. Scarborough, M. J., Lawson, C. E., DeCola, A. C. & Gois, I. M. Microbiomes for sustainable biomanufacturing. *Curr. Opin. Microbiol.* **65**, 8–14 (2022).
2. Stamatopoulou, P., Malkowski, J., Conrado, L., Brown, K. & Scarborough, M. Fermentation of Organic Residues to Beneficial Chemicals: A Review of Medium-Chain Fatty Acid Production. *Processes* **8**, 1571 (2020).
3. Angenent, L. T. *et al.* Chain Elongation with Reactor Microbiomes: Open-Culture Biotechnology To Produce Biochemicals. *Environ. Sci. Technol.* **50**, 2796–2810 (2016).

832 4. Harvey, B. G. & Meylemans, H. A. 1-Hexene: a renewable C6 platform for full-performance jet and
833 diesel fuels. *Green Chem* **16**, 770–776 (2014).
834 5. Urban, C. *et al.* Production of drop-in fuels from biomass at high selectivity by combined microbial
835 and electrochemical conversion. *Energy Environ. Sci.* **10**, 2231–2244 (2017).
836 6. Rosa, L. F. M., Röhring, K. & Harnisch, F. Electrolysis of medium chain carboxylic acids to aviation
837 fuel at technical scale. *Fuel* **356**, 129590 (2024).
838 7. Battista, F. & Bolzonella, D. Beyond Anaerobic Digestion: New Perspectives for the Development
839 of a Biorefinery Platform for the Simultaneous Production of Medium-Chain Fatty Acids by
840 Chain Elongation and Biogas from Food Wastes. *ACS Sustain. Chem. Eng.* **12**, 15294–15306
841 (2024).
842 8. Agena, E. *et al.* Evaluating the feasibility of medium-chain oleochemical synthesis using microbial
843 chain elongation. *J. Ind. Microbiol. Biotechnol.* **51**, kuae027 (2024).
844 9. Tarasava, K. *et al.* Reverse β-oxidation pathways for efficient chemical production. *J. Ind.*
845 *Microbiol. Biotechnol.* **49**, kuac003 (2022).
846 10. Barker, H. A. Clostridium Kluyveri. *Antonie Van Leeuwenhoek* **12**, 167–176 (1947).
847 11. Spirito, C. M., Richter, H., Rabaey, K., Stams, A. J. & Angenent, L. T. Chain elongation in
848 anaerobic reactor microbiomes to recover resources from waste. *Curr. Opin. Biotechnol.* **27**,
849 115–122 (2014).
850 12. Duncan, S. H., Barcenilla, A., Stewart, C. S., Pryde, S. E. & Flint, H. J. Acetate Utilization and
851 Butyryl Coenzyme A (CoA):Acetate-CoA Transferase in Butyrate-Producing Bacteria from the
852 Human Large Intestine. *Appl. Environ. Microbiol.* **68**, 5186–5190 (2002).
853 13. Hesser, L. A. *et al.* A synbiotic of Anaerostipes caccae and lactulose prevents and treats food allergy
854 in mice. *Cell Host Microbe* **32**, 1163-1176.e6 (2024).
855 14. Liu, D. *et al. Anaerostipes hadrus* , a butyrate-producing bacterium capable of metabolizing 5-
856 fluorouracil. *mSphere* **9**, e00816-23 (2024).

857 15. Notting, F., Pirovano, W., Sybesma, W. & Kort, R. The butyrate-producing and spore-forming
858 bacterial genus *Coprococcus* as a potential biomarker for neurological disorders. *Gut Microbiome*
859 **4**, e16 (2023).
860 16. Hillman, E. T. *et al.* Comparative genomics of the genus Roseburia reveals divergent biosynthetic
861 pathways that may influence colonic competition among species. *Microb. Genomics* **6**, (2020).
862 17. Scarborough, M. J., Myers, K. S., Donohue, T. J. & Noguera, D. R. Medium-Chain Fatty Acid
863 Synthesis by " *Candidatus* Weimeria bifida" gen. nov., sp. nov., and " *Candidatus*
864 Pseudoramibacter fermentans" sp. nov. *Appl. Environ. Microbiol.* **86**, e02242-19 (2020).
865 18. Thauer, R. K., Jungermann, K., Henninger, H., Wenning, J. & Decker, K. The Energy Metabolism of
866 *Clostridium kluyveri*. *Eur. J. Biochem.* **4**, 173–180 (1968).
867 19. Thauer, R. K., Jungermann, K., Rupprecht, E. & Decker, K. Hydrogen formation from NADH in
868 cell-free extracts of *Clostridium kluyveri*: Acetyl coenzyme A requirement and ferredoxin
869 dependence. *FEBS Lett.* **4**, 108–112 (1969).
870 20. Jungermann, K., Thauer, R. K., Rupprecht, E., Ohrloff, C. & Decker, K. Ferredoxin mediated
871 hydrogen formation from NADPH in a cell-free system of *Clostridium kluyveri*. *FEBS Lett.* **3**,
872 144–146 (1969).
873 21. Li, F. *et al.* Coupled Ferredoxin and Crotonyl Coenzyme A (CoA) Reduction with NADH Catalyzed
874 by the Butyryl-CoA Dehydrogenase/Etf Complex from *Clostridium kluyveri*. *J. Bacteriol.* **190**,
875 843–850 (2008).
876 22. Buckel, W. & Thauer, R. K. Energy conservation via electron bifurcating ferredoxin reduction and
877 proton/Na+ translocating ferredoxin oxidation. *Biochim. Biophys. Acta BBA - Bioenerg.* **1827**,
878 94–113 (2013).
879 23. Wang, S., Huang, H., Moll, J. & Thauer, R. K. $NADP^+$ Reduction with Reduced Ferredoxin and
880 $NADP^+$ Reduction with NADH Are Coupled via an Electron-Bifurcating Enzyme Complex in
881 *Clostridium kluyveri*. *J. Bacteriol.* **192**, 5115–5123 (2010).

882 24. Seedorf, H. *et al.* The genome of Clostridium kluyveri, a strict anaerobe with unique metabolic
883 features. *Proc. Natl. Acad. Sci.* **105**, 2128–2133 (2008).
884 25. Shetty, S. A., Boeren, S., Bui, T. P. N., Smidt, H. & De Vos, W. M. Unravelling lactate-acetate and
885 sugar conversion into butyrate by intestinal *Anaerobutyricum* and *Anaerostipes* species by
886 comparative proteogenomics. *Environ. Microbiol.* **22**, 4863–4875 (2020).
887 26. Kattel, A. *et al.* Detailed analysis of metabolism reveals growth-rate-promoting interactions between
888 Anaerostipes caccae and Bacteroides spp. *Anaerobe* **79**, 102680 (2023).
889 27. Louis, P., Duncan, S. H., Sheridan, P. O., Walker, A. W. & Flint, H. J. Microbial lactate utilisation
890 and the stability of the gut microbiome. *Gut Microbiome* **3**, e3 (2022).
891 28. Crognale, S. *et al.* Ecology of food waste chain-elongating microbiome. *Front. Bioeng. Biotechnol.*
892 **11**, 1157243 (2023).
893 29. Crognale, S. *et al.* Direct Conversion of Food Waste Extract into Caproate: Metagenomics
894 Assessment of Chain Elongation Process. *Microorganisms* **9**, 327 (2021).
895 30. Wang, Y., Qiu, J., Lü, F., Zhang, H. & He, P.-J. Lactate to caproate chain elongation: Kinetic
896 characterization and theoretical model for real-time monitoring. *Chem. Eng. J.* **524**, 169236
897 (2025).
898 31. Liu, B., Kleinsteuber, S., Centler, F., Harms, H. & Sträuber, H. Competition Between Butyrate
899 Fermenters and Chain-Elongating Bacteria Limits the Efficiency of Medium-Chain Carboxylate
900 Production. *Front. Microbiol.* **11**, 336 (2020).
901 32. Afzal, M. X., Bonatelli, M. L., Kleinsteuber, S., Sträuber, H. & Baleeiro, F. C. F. Reduced carbon
902 emissions and chain elongation during mixotrophic fermentation of a biomass feedstock.
903 33. Luo, Y. *et al.* Process innovation for caproate production at neutral pH: Development and
904 characterization of a novel Anaerococcus-centered microbial community converting lactate to
905 caproate. *Chem. Eng. J.* **524**, 169607 (2025).

906 34. Tang, J. *et al.* Caproic acid production through lactate-based chain elongation: Effect of lactate-to-
907 acetate ratio and substrate loading. *Environ. Technol. Innov.* **28**, 102918 (2022).
908 35. Yin, Y., Zhang, Y., Karakashev, D. B., Wang, J. & Angelidaki, I. Biological caproate production by
909 Clostridium kluyveri from ethanol and acetate as carbon sources. *Bioresour. Technol.* **241**, 638–
910 644 (2017).
911 36. Wang, H., Zhou, W., Gao, J., Ren, C. & Xu, Y. Revealing the Characteristics of Glucose- and
912 Lactate-Based Chain Elongation for Caproate Production by *Caproicibacterium*
913 *lactatifermentans* through Transcriptomic, Bioenergetic, and Regulatory Analyses. *mSystems* **7**,
914 e00534-22 (2022).
915 37. Smith, G. M., Kim, B. W., Franke, A. A. & Roberts, J. D. 13C NMR studies of butyric fermentation
916 in Clostridium kluyveri. *J. Biol. Chem.* **260**, 13509–13512 (1985).
917 38. Spirito, C. M. *et al.* Variability in n-caprylate and n-caproate producing microbiomes in reactors with
918 in-line product extraction. *mSystems* **9**, e00416-24.
919 39. Gildemyn, S. *et al.* Upgrading syngas fermentation effluent using Clostridium kluyveri in a
920 continuous fermentation. *Biotechnol. Biofuels* **10**, 83 (2017).
921 40. Schoberth, S. & Gottschalk, G. Considerations on the energy metabolism of Clostridium kluyveri.
922 *Arch. F□r Mikrobiol.* **65**, 318–328 (1969).
923 41. Sliwkowski, M. X. & Hartmanis, M. G. N. Simultaneous single-step purification of thiolase and
924 NADP-dependent 3-hydroxybutyryl-CoA dehydrogenase from *Clostridium kluyveri*. *Anal.*
925 *Biochem.* **141**, 344–347 (1984).
926 42. Noor, E. *et al.* Pathway Thermodynamics Highlights Kinetic Obstacles in Central Metabolism. *PLoS*
927 *Comput. Biol.* **10**, e1003483 (2014).
928 43. Flamholz, A., Noor, E., Bar-Even, A., Liebermeister, W. & Milo, R. Glycolytic strategy as a tradeoff
929 between energy yield and protein cost. *Proc. Natl. Acad. Sci.* **110**, 10039–10044 (2013).

930 44. Flamholz, A. I., Goyal, A., Fischer, W. W., Newman, D. K. & Phillips, R. The proteome is a
931 terminal electron acceptor. 2024.01.31.578293 Preprint at
932 https://doi.org/10.1101/2024.01.31.578293 (2024).
933 45. McMahon, M. D. & Prather, K. L. J. Functional Screening and *In Vitro* Analysis Reveal
934 Thioesterases with Enhanced Substrate Specificity Profiles That Improve Short-Chain Fatty Acid
935 Production in Escherichia coli. *Appl. Environ. Microbiol.* **80**, 1042–1050 (2014).
936 46. Jindra, M. A. *et al.* Evaluation of strategies to narrow the product chain-length distribution of
937 microbially synthesized free fatty acids. *Metab. Eng.* **77**, 21–31 (2023).
938 47. Yang, Q. *et al.* Butyryl/Caproyl-CoA:Acetate CoA-transferase: cloning, expression and
939 characterization of the key enzyme involved in medium-chain fatty acid biosynthesis. *Biosci.*
940 *Rep.* **41**, BSR20211135 (2021).
941 48. Charrier, C. *et al.* A novel class of CoA-transferase involved in short-chain fatty acid metabolism in
942 butyrate-producing human colonic bacteria. *Microbiology* **152**, 179–185 (2006).
943 49. Hackmann, T. J. Redefining the coenzyme A transferase superfamily with a large set of manually
944 annotated proteins. *Protein Sci.* **31**, 864–881 (2022).
945 50. Barker, H. A. & Barker, H. A. *Bacterial Fermentations*. (Wiley, New York, 1956).
946 doi:10.5962/bhl.title.7301.
947 51. Barker, H. A. & Taha, S. M. Clostridium kluyverii, an organism concerned in the formation of
948 caproic acid from ethyl alcohol. *J. Bacteriol.* **43**, 347–363 (1942).
949 52. Bornstein, B. T. & Barker, H. A. The Nutrition of *Clostridium kluyveri*. *J. Bacteriol.* **55**, 223–230
950 (1948).
951 53. Allaart, M. T. *et al.* Physiological and stoichiometric characterization of ethanol-based chain
952 elongation in the absence of short-chain carboxylic acids. *Sci. Rep.* **13**, 17370 (2023).

953 54. Spirito, C. M., Marzilli, A. M. & Angenent, L. T. Higher Substrate Ratios of Ethanol to Acetate
954 Steered Chain Elongation toward *n* -Caprylate in a Bioreactor with Product Extraction. *Environ.*
955 *Sci. Technol.* **52**, 13438–13447 (2018).
956 55. Esquivel-Elizondo, S. *et al.* The Isolate Caproiciproducens sp. 7D4C2 Produces n-Caproate at
957 Mildly Acidic Conditions From Hexoses: Genome and rBOX Comparison With Related Strains
958 and Chain-Elongating Bacteria. *Front. Microbiol.* **11**, (2021).
959 56. de Leeuw, K. D. *et al.* Methanol-Based Chain Elongation with Acetate to n-Butyrate and Isobutyrate
960 at Varying Selectivities Dependent on pH. *ACS Sustain. Chem. Eng.* **8**, 8184–8194 (2020).
961 57. Chen, W. S., Ye, Y., Steinbusch, K. J. J., Strik, D. P. B. T. B. & Buisman, C. J. N. Methanol as an
962 alternative electron donor in chain elongation for butyrate and caproate formation. *Biomass*
963 *Bioenergy* **93**, 201–208 (2016).
964 58. Zhang, Y., Liu, B., Wu, W., Liu, H. & Wang, W. Propanol as electron donor for efficient odd-chain
965 carboxylate production by chain elongation with reactor microbiomes. *J. Environ. Sci.* **156**, 849–
966 858 (2025).
967 59. Vögeli, B. *et al.* Cell-free prototyping enables implementation of optimized reverse β-oxidation
968 pathways in heterotrophic and autotrophic bacteria. *Nat. Commun.* **13**, 3058 (2022).
969 60. Jeon, B. S. *et al.* Molecular Chain Elongation Mechanism for *n* -Caproate Biosynthesis by
970 *Megasphaera Hexanoica*. *Adv. Sci.* e06069 (2025) doi:10.1002/advs.202506069.
971 61. Mann, M. S. & Lütke-Eversloh, T. Thiolase engineering for enhanced butanol production in
972 Clostridium acetobutylicum. *Biotechnol. Bioeng.* **110**, 887–897 (2013).
973 62. Hu, L. *et al.* Rex in Clostridium kluyveri is a global redox-sensing transcriptional regulator. *J.*
974 *Biotechnol.* **233**, 17–25 (2016).
975 63. Wietzke, M. & Bahl, H. The redox-sensing protein Rex, a transcriptional regulator of
976 solventogenesis in Clostridium acetobutylicum. *Appl. Microbiol. Biotechnol.* **96**, 749–761
977 (2012).

978 64. McCleary, W. R., Stock, J. B. & Ninfa, A. J. Is acetyl phosphate a global signal in Escherichia coli?
979 *J. Bacteriol.* **175**, 2793–2798 (1993).
980 65. Gao, R., Mack, T. R. & Stock, A. M. Bacterial response regulators: versatile regulatory strategies
981 from common domains. *Trends Biochem. Sci.* **32**, 225–234 (2007).
982 66. Wolfe, A. J. The Acetate Switch. *Microbiol. Mol. Biol. Rev.* **69**, 12–50 (2005).
983 67. Wang, Q. *et al.* Acetylation of Metabolic Enzymes Coordinates Carbon Source Utilization and
984 Metabolic Flux. *Science* **327**, 1004–1007 (2010).
985 68. Weinert, B. T. *et al.* Acetyl-Phosphate Is a Critical Determinant of Lysine Acetylation in E. coli.
986 *Mol. Cell* **51**, 265–272 (2013).
987 69. Willems, A. & Collins, M. D. Phylogenetic Relationships of the Genera Acetobacterium and
988 Eubacterium Sensu Strict0 and Reclassification of Eubacterium alactolyticum as
989 Pseudoramibacter alactolyticus gen. nov., comb. nov.
990 70. Bernatchez, J. A. & McCall, L.-I. Insights gained into respiratory infection pathogenesis using lung
991 tissue metabolomics. *PLOS Pathog.* **16**, e1008662 (2020).
992 71. Kozioł, A., Pupek, M. & Lewandowski, Ł. Application of metabolomics in diagnostics and
993 differentiation of meningitis: A narrative review with a critical approach to the literature. *Biomed.*
994 *Pharmacother.* **168**, 115685 (2023).
995 72. Hojo, S., Komatsu, M., Okuda, R., Takahashi, N. & Yamada, T. Acid Profiles and pH of Carious
996 Dentin in Active and Arrested Lesions. *J. Dent. Res.* **73**, 1853–1857 (1994).
997 73. Mortensen, P. B. & Clausen, M. R. Short-Chain Fatty Acids in the Human Colon: Relation to
998 Gastrointestinal Health and Disease. *Scand. J. Gastroenterol.* **31**, 132–148 (1996).
999 74. Bose, S., Ramesh, V. & Locasale, J. W. Acetate Metabolism in Physiology, Cancer, and Beyond.
1000 *Trends Cell Biol.* **29**, 695–703 (2019).
1001 75. Wang, S. P. *et al.* Pivotal Roles for pH, Lactate, and Lactate-Utilizing Bacteria in the Stability of a
1002 Human Colonic Microbial Ecosystem. *mSystems* **5**, e00645-20 (2020).

1003 76. Macfarlane, G. T., Gibson, G. R. & Cummings, J. H. Comparison of fermentation reactions in
1004 different regions of the human colon. *J. Appl. Bacteriol.* **72**, 57–64 (1992).
1005 77. Liu, Y., Lü, F., Shao, L. & He, P. Alcohol-to-acid ratio and substrate concentration affect product
1006 structure in chain elongation reactions initiated by unacclimatized inoculum. *Bioresour. Technol.*
1007 **218**, 1140–1150 (2016).
1008 78. Brodowski, F., Łężyk, M., Gutowska, N. & Oleskowicz-Popiel, P. Effect of external acetate on
1009 lactate-based carboxylate platform: Shifted lactate overloading limit and hydrogen co-production.
1010 *Sci. Total Environ.* **802**, 149885 (2022).
1011 79. Liu, B., Kleinsteuber, S., Centler, F., Harms, H. & Sträuber, H. Competition Between Butyrate
1012 Fermenters and Chain-Elongating Bacteria Limits the Efficiency of Medium-Chain Carboxylate
1013 Production. *Front. Microbiol.* **11**, 336 (2020).
1014 80. Lawson, C. E. Retooling Microbiome Engineering for a Sustainable Future. *mSystems* **6**,
1015 10.1128/msystems.00925-21 (2021).
1016 81. Lawson, C. E. *et al.* Investigating the Chemolithoautotrophic and Formate Metabolism of Nitrospira
1017 moscoviensis by Constraint-Based Metabolic Modeling and ^{13}C-Tracer Analysis. *mSystems* **6**,
1018 10.1128/msystems.00173-21 (2021).
1019 82. Keller, A., Nesvizhskii, A. I., Kolker, E. & Aebersold, R. Empirical Statistical Model To Estimate
1020 the Accuracy of Peptide Identifications Made by MS/MS and Database Search. *Anal. Chem.* **74**,
1021 5383–5392 (2002).
1022 83. Nesvizhskii, A. I., Keller, A., Kolker, E. & Aebersold, R. A Statistical Model for Identifying
1023 Proteins by Tandem Mass Spectrometry. *Anal. Chem.* **75**, 4646–4658 (2003).
1024 84. Sato, M. *et al.* Three CoA Transferases Involved in the Production of Short Chain Fatty Acids in
1025 Porphyromonas gingivalis. *Front. Microbiol.* **07**, (2016).
1026 85. Noor, E., Haraldsdóttir, H. S., Milo, R. & Fleming, R. M. T. Consistent Estimation of Gibbs Energy
1027 Using Component Contributions. *PLoS Comput. Biol.* **9**, e1003098 (2013).

1028 86. Bennett, B. D. *et al.* Absolute metabolite concentrations and implied enzyme active site occupancy
1029 in Escherichia coli. *Nat. Chem. Biol.* **5**, 593–599 (2009).
1030 87. Vizcaíno, J. A. *et al.* The Proteomics Identifications (PRIDE) database and associated tools: status in
1031 2013. *Nucleic Acids Res.* **41**, D1063–D1069 (2012).
1032